Received: 29 August 2023 | Revised: 7 December 2023 | Accepted: 22 December 2023

IET Power Electronics

DOI: 10.1049/pel2.12647

The Institution of Engineering and Technology WILEY

ORIGINAL RESEARCH

Comparative analysis of three-phase dual active bridge converter with different transformer topology and modern universal control for DC microgrids

Serafin Bachman[1] | **Marek Turzyński**[2] | **Marek Jasiński**[1]

[1]Institute of Control and Industrial Electronics, Warsaw University of Technology, Warsaw, Poland

[2]Faculty of Electrical and Control Engineering, Gdansk University of Technology, Gdańsk, Poland

Correspondence
Serafin Bachman, Institute of Control and Industrial Electronics, Warsaw University of Technology, 00-843 Warsaw, Poland.
Email: serafin.bachman@pw.edu.pl

Abstract

The presented work discusses issues related to the use of modern multiphase topologies of Dual Active Bridge (DAB)-type converters. Converters of this type are widely used in most DC microgrid applications. The introduction emphasizes a comparative analysis between single-phase and multi-phase DAB topologies within high-power DC microgrids, delving into their respective advantages, drawbacks, design procedures, and considerations based on the latest knowledge. The publication explores the comparison and selection of viable topologies for deployment in high-power and high-efficiency DC microgrids. The unified method of controlling 1-phase and multi-phase DAB converters was proposed in this design, simplifying the issues of DC microgrid control. All topologies were tested on the same controller concept. The study performs laboratory investigation of DAB 1-phase and 3-phase: Star–Star, and Star–Delta topologies. Attention was paid to maintaining uniform operating conditions of the system, contrary to studies known from the literature, all tests were carried out on the same laboratory stand and the same magnetic components in different configurations. Analytical and laboratory analyses of the Zero Voltage Switching (ZVS) region were performed, accounting for non-linear phenomena. Based on these findings, an assessment of the system's performance in soft switching was carried out. The presented results were implemented in a simulation model and subsequently validated through tests on a constructed laboratory setup to ensure the proper operation of the system. This work meticulously presents and discusses variations in efficiency, dynamic response, phase current harmonic distribution, phase shift distribution, ZVS switching region, and more among the examined topologies. To ensure a fair comparison, the converter configuration for both simulation and laboratory models utilized identical components across all configurations.

1 | INTRODUCTION

The dissemination of the microgrid concept has a significant impact on the current appearance of energy infrastructure. This concept involves combining AC and DC installations into a coherent whole to adapt to the needs of various solutions in the field of electrical engineering developed around the world. In a DC microgrid, electricity is generated by various sources such as photovoltaic panels, wind turbines, batteries, generators etc. This energy is then stored and distributed directly in the form of direct current, eliminating the need for conversion to alternating current. Energy losses associated with the conversion of energy by the next stage are thus avoided. This concept also enables use of electronic devices and systems that are characterized by high efficiency. It is a field of the future, interdisciplinary, and currently implemented around the world. In this publication, we will focus on the DC microgrid part.

A very important part of the DC network is a possibility of energy conversion for high-power installations. The key aspect of such an application is to ensure high efficiency and safety. For

these reasons and many others, the most popular topology currently used in DC microgrids is the Dual Active Bridge (DAB) converter. It provides the ability to transfer energy between systems with different potentials while maintaining high efficiency of up to 98% [1].

High-power microgrid installations find applications in various domains such as photovoltaic installations, electric vehicle charging systems, and smart energy storage systems. All these installations focus on the safe transmission of high energy. The energy density of power electronic converters is limited by available semiconductor and magnetic elements. For this reason, multi-phase and/or parallel systems are used. DAB is a universal topology that allows the converters to be connected in any way; however, it is burdened with a problem of circulating currents [2].

An alternative proposition involves the use of multi-phase systems like DAB 3-phase topologies [3], which can be connected in series-parallel configurations akin to the classic DAB topology [4, 5]. Such solutions are prevalent in medium-power systems, offering higher peak power than the traditional topology.

Multi-phase topologies may vary in terms of the implementation of magnetic components [6] or semiconductor topologies [7]. Despite differences in construction cost and achievable energy density, these solutions operate in a fundamentally similar manner. For this reason, this publication will discuss a comparison of topologies differing in the configuration of transformer winding while maintaining the classic semiconductor topology in the form of a classic three-phase bridge.

Presently, control methods for 3-phase DAB converters primarily aim at extending the Zero Voltage Switching (ZVS) range [8–10] or involve strategies for detecting emergency states [11]. These control approaches leverage various modulators, ranging from fundamental Single-Phase Shift (SPS) to more sophisticated methods like those discussed in [12–15], all relying on either current or voltage–current control loops. However, such solutions lack the desired flexibility, limiting their applicability across a diverse range of scenarios.

The literature explores numerous modulators suitable for 3-phase DAB systems, yet a comprehensive modulation strategy remains not solved. In contrast to 1-phase DAB systems, conventional modulation methods such as Dual Phase Shift (DPS) and Triple Phase Shift (TPS) are not compatible with 3-phase setups. The distinct structure of the three-phase bridge prohibits the utilization of the same equations and relationships employed in the single-phase system [14].

Modifications of the classic SPS modulation, incorporating additional parameters like duty cycle control (DCC) [13], have gained traction for enhancing system performance in dynamic states and improving efficiency at varying voltage ratios. Simultaneous Pulse Width Modulation (SPWM) is another widely adopted approach [13], while some researchers delve into fully predictive control methods [14]. Another interesting method is [13] fast transient current control (FTCC) method for the 3p-DAB with variable duty cycles. However, these advanced solutions pose implementation challenges, demanding substantial computational power from the control system. Notably, these studies often overlook important aspects related to control loop dynamics and flexibility.

The existing literature features several works that explore the comparison between 1-phase and 3-phase DAB topologies [15]. However, these studies often overlook the consideration of diverse transformer topologies and fail to account for operations on identical magnetic components. Moreover, they lack a comprehensive analysis of current harmonics across the evaluated topologies.

A work as [17] addresses the comparison of transformer current harmonics. Nevertheless, the investigation in [17] is conducted exclusively on multi-level topologies, and examinations across the same magnetic circuit are notably absent.

Several research articles, namely [12, 16, 29–36], offer insights into various topologies. Despite this, there remains a notable absence of a cohesive presentation delineating the distinctions between these topologies in a singular work, without introducing hardware variations.

Furthermore, a comparative study of different transformer topology variants is discussed in [9]. Regrettably, this comparison fails to present findings related to harmonic distribution. The study lacks assessments at low frequencies, does not include a comparison to a single-phase system, and overlooks the consideration of dynamic states in its analyses.

The contribution of this publication is to carry out comprehensive analytical and laboratory tests of the 3-phase DAB system in two transformer configurations. A comparison of results with a 1-phase system operates in the same conditions. Investigations are made in accordance with novel research. Conduct research using the original universal control loop used for all solutions. Carry out a detailed analysis of ZVS state for Star–Star and Star–Delta topology. Comparison of differences between transformer topologies in terms of efficiency, dynamic states, starting currents, and phase current harmonics, while maintaining the same magnetic circuit, contrary to studies known from the literature. In essence, this article stands as a valuable supplement to existing bibliographic items, contributing a unique perspective and expanding the current understanding within the field.

2 | TOPOLOGY COMPARISON

The most common DAB topology is single-phase. Its scheme is presented in Figure 1a. It is compared in Table 1 with the 3-phase DAB converter with transformer star-star topology shown in Figure 2b. Both topologies have similar properties and applications, but the difference is hidden in the details. DAB 1-phase converters are used very widely and, depending on the design, they can be used in medium power and medium voltage systems [7, 17, 18].

Multi-phase topologies are mainly found in higher-power applications, for power higher than 10 kW [17–20]. A comparison of the schematic of DAB 1-phase versus DAB 3-phase topology scheme is shown in Figure 1.

TABLE 1 Comparison of properties of DAB-1 phase.

Properties	DAB-1 phase	DAB-3 phase
Price	Less expensive	More expensive
Number of transistors	8	12 (2 × 3 ph-FB) or 16 (4x FB)
Magnetic circuit	Less complicated	Complicated 3 phase transf. and 3 inductors
Number of elements	Only 2x FB and magnetics	More components
Dynamic states	Faster dynamic(∼100 us)[a]	Slower dynamic(∼200 us)[a]
DC offset problem	Bigger asymmetry currents	Smaller asymmetry currents
Inrush starting current	Very big (possible 100 A+)[a]	Approximately 1/3 of DAB 1-phase
Peak power	Depends on design	1.5 times of DAB 1-phase
Energy density	Normal	Higher
Current shape	Trapezoidal (∼20 A/5 kW)[a]	Sinusoidal (∼10 A/5 kW)[a]
EMI	Very high	Less than DAB 1-phase
Control	Classic phase shift equation	More complex phase shift equation
Efficiency	Max 98%[a]	Max 97%[a]

DAB, dual active bridge.
[a]Results obtained during laboratory tests Vin = 690 V, Vout = 380 V, Pmax = 10 kW, Fs = 50 kHz.

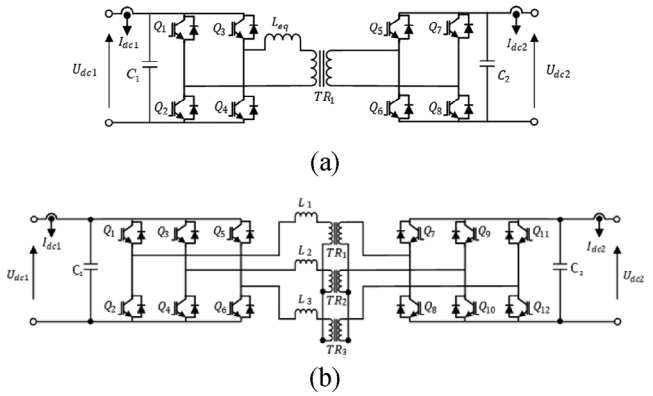

FIGURE 1 This figure presents DAB topologies: (a) DAB 1-phase, (b) DAB-3 phase. DAB, dual active bridge.

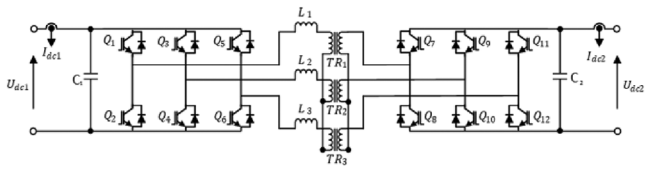

FIGURE 2 This figure presents DAB 3-phase in Star–Star transformer topology. DAB, dual active bridge.

Changing the single-phase system to a three-phase system involves significant complexity of the magnetic circuit; its complexity has been discussed in [21].

The topology comparison [22–24] presented in Table 1 shows the superiority of the DAB 3-phase system for high-power systems. The comparison depends on the particular converter design specified in Table 1 [1], the results may vary depending on design.

For further work, the DAB 3-phase topology was selected. It is characterized by a higher peak power, which determines its choice for use in high-power applications while maintaining lower problems. Other variants of the DAB topology such as the parallel connection of DAB 1-phase are not considered as an application in this publication due to problems with the currents circulating between the modules. In the following section, we will focus on topology variants of the 3-phase DAB.

3 | ANALYSIS OF 3-PHASE DUAL ACTIVE BRIDGE VARIANTS

DAB 3-phase can be divided into magnetic component variants:

(1) Common magnetic core
(2) Separate transformer design for each phase
(3) Topology Star–Star
(4) Topology Star–Delta
(5) Other configurations

The 3-phase DAB can have a design with a common or split magnetic core transformer [18], the efficiency of which depends on the design. It is assumed that transformers with a common core have a much higher price and slightly a higher efficiency [17]; however, results can vary depending on the design. The type of winding connection in a three-phase system depends on the designer and the expected results as well as exemplary topologies are discussed in [17–24]. The most popular topologies are Star–Star and Star–Delta. Other transformer variants are not as common and therefore will not be discussed. Another possible division of 3-phase DAB is based on semiconductor topology [25, 26]. The classic solution is to use two compact

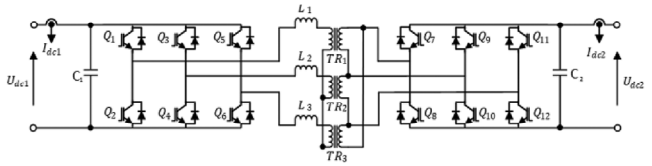

FIGURE 3 This figure presents DAB 3-phase in Star–Delta transformer topology. DAB, dual active bridge.

3-phase bridges or 6-separate half bridges [27]. However, it is also possible to use six single-phase bridges [28] with separate transformers for each phase. This solution significantly increases the cost of the entire converter and reduces the potential energy density, but increases peak transfer power. Based on [29], it was assumed that the Star–Delta and Delta–Star topologies work analogously for a system with a voltage ratio equal to one.

For further analysis, the Star–Star and Star–Delta topologies with the split transformer, using two complex semiconductor 3-phase bridges, were selected due to their modularity, price, and non-exhaustive discussion in the literature.

3.1 | Star–star

The topology diagram is shown in Figure 2.

This topology is characterized by:

- Star–Star having a wider allowed range of voltage ratio for higher power load [29]
- Same phase and line current for the transformer [30]
- Low efficiency for low loads [30]
- Higher peak efficiency [19]
- Lower RMS currents than Star–Delta topology [30]
- Less sinusoidal phase current shape [32]
- Lower series inductance value [33]
- Lower phase shift angle than in the Star–Delta topology at the same load [34]
- For phase shift equal π losses ZVS condition [35]
- The topology is intended for use in high-power systems with a small range of voltage variability [36]

3.2 | Star–delta

The topology diagram is shown in Figure 3.

This topology is characterized by:

- DC link capacitance being able to be reduced by 40% compared to Star–Star topology [17]
- The Star–Delta type conventional DAB suffering from a low efficiency and low transformer utilization in partial loads, as shown in the study [17]
- The converter with the Star–Delta winding configuration having higher current harmonics in partial loads than the Star–Star configuration—with the fifth and the seventh being the dominant harmonics. It has also been shown that these harmonics contribute positively to the power flow of the Star–Star configuration. On the contrary, the active power flow direction of the harmonics is the opposite of the fundamental for the Star–Delta configuration. This results in the poor harmonic performance of the Star–Delta configuration at low loads and potentially can result in increased losses [30]
- Star–Delta having a wider range of the allowed voltage ratio, at no load or light load conditions [30]
- Increase of ZVS region for power levels below 30% [30]
- Low efficiency for low loads [31]
- More sinusoidal phase current shape—less THDi [32]
- Higher series inductance compared to Star–Star [33]
- Higher possible voltage ratio (from laboratory tests Star–Star 1,5 ratio, Star–Delta 1,8 [34]
- For power levels between 30 and 80%, a lower switch turn-off current can be seen for the Star–Delta configuration [34]
- Secondary side current is reduced by factor $\sqrt{3}$ [35]
- In practice, ZVS boundaries are impacted by the parasitic capacitance of the switches and dead time. As a result, the soft switching boundary is slightly changed.
- Less reactive power flow in AC phase side [35]
- The topology works better for applications involving wide-range voltage changes [35]

4 | CONTROL LOOP

The aim of this paper is to consider a fully universal 3-phase DAB system with various transformer topologies. Thus the control loop provides an immediate change between control of the set value: current, voltage, and power. Moreover, there is a safe and simple transition in control states, especially in states of dynamic changes in load impedance. Furthermore, please note that the control loop is intended for both Star–Star and Star–Delta topologies.

The block for selecting the correct regulation value is implemented based on the selection of the smallest calculated instantaneous set current value, which minimizes the problem of switching between regulation states.

A diagram of the control loop used in the DAB 3-phase control is presented in Figure 4. The control topology was already proposed by the authors in other publications for the operation of the system with the 1-phase DAB topology [36, 37]. This control is characterized by universality of operation for DAB-type converters. It only requires modification of the phase shift equation for the appropriate converter variant. When calculating the equation, it is important to take into account the non-linearity of DAB converters and problems with dead time drift; this topic is discussed in [32]. The control loop must involve Equations (1) and (2). The modulator should also be matched to the topology variant.

To ensure that controllers can be switched safely, these controllers start together with the same settings. Moreover, when changing the controller, the integral value is transferred to the second controller. In addition, the setpoint passes through a

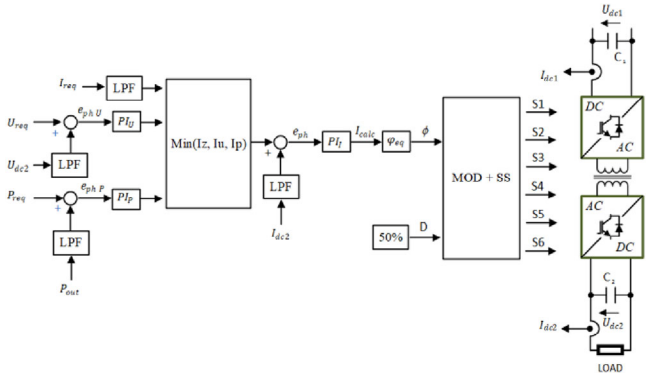

FIGURE 4 Control loop of DAB 3-phase. DAB, dual active bridge.

low pass filter, limiting its initial dynamics when changing the controller, in first transition.

The control loop consists of a modulator with an additional phase shift between the gate signals for the first control pulses to reduce the current asymmetry phenomenon of the converter. The value of the set current is calculated on the basis of the phase shift equation, derived from Equations (1) and (2). The control loop can be selected as a closed current, current-voltage, or current-power loop. The system is tuned on the basis of the principle discussed in another publication by the authors [38].

The source of the derivation of the power equation used in the DAB 3-phase converter is [26]. The applied power equation is presented below:

$$\varphi = \frac{1}{2} - \sqrt{\frac{1}{4} - \frac{2NLF_{sw}P_{out}}{V_{in}V_{out}}},\ if\ i_0 > 0 \tag{1}$$

$$\varphi = -\frac{1}{2} + \sqrt{\frac{1}{4} + \frac{2NLF_{sw}P_{out}}{V_{in}V_{out}}},\ if\ i_0 \le 0 \tag{2}$$

Series inductance calculation is based on the phase shift equation and presented below:

$$L_1 = L_2 = L_3 = \frac{7nV_{in}V_{out}}{8F_{sw}P_{max}} \tag{3}$$

where φ is the phase shift, N the voltage ratio, L the leakage inductance of one phase, F_{sw} the switching frequency, P_{out} the output power, i_0 the phase current, $V_{in}V_{out}$ the input and output voltages and P_{max} the maximum output power of the converter.

Due to the application of the two transformer topologies and the differences in the transformer ratio, it was necessary to fine tune the PI controllers. A detailed discussion of the calculation of the converter settings is presented in [38]. The obtained results of PI settings are presented in Table 2.

5 | LABORATORY SETUP

The layout of the stand is presented in Figure 5. The system is tested using two independent DC power supplies by

TABLE 2 Comparison of PI control tuning parameters for Star–Star and Star–Delta topologies.

Properties	Star–Star	Star–Delta
Kp	0.5	0.75
Ki	0.5	0.75
Ti	0.0008	0.00055
Tf	$6.82 \times 10 \times 10^{-3}$	$6.82 \times 10 \times 10^{-3}$
Kf	$5.86 \times 10 \times 10^{-4}$	$5.86 \times 10 \times 10^{-4}$

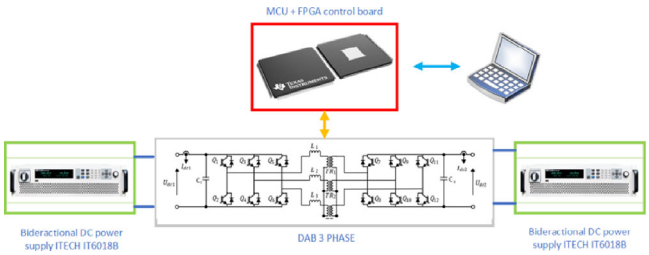

FIGURE 5 Laboratory setup based on bidirectional DC power supply.

TABLE 3 Laboratory setup parameters of DAB 3-phase.

Properties	Specification
Rated output power	10 kW
Udc1	600 V/380 V
Udc2	324 V
Switching frequency	50 kHz
Power supply	ITECH60188
Transformer	3 × 3C95 ferrite core (SMA) OD = 87/ID = 56/H = 50 mm
L1, L2, L3	25 μH
Power supply	ITECH60188
Efficiency meter	Yokogawa WT5000
Transistors	F423MR12W1M1PB11BPSA1

DAB, dual active bridge.

ITECH IT6018B and adjustable ITACH load. The microcontroller (MCU) and field programmable gate array (FPGA) control board, connected through the JTAG to the computer, controls the converter and auxiliary agents.

The laboratory setup parameters for both topologies are presented in Table 3.

The test laboratory setup pictures are presented in Figure 6.

6 | LABORATORY RESULTS

The results obtained on the laboratory setup are presented below, divided into static, dynamic, efficiency, and switching characteristic results.

Figure 7 presents the static results of the Star–Star topology, the most interesting part of the characteristic being the shape

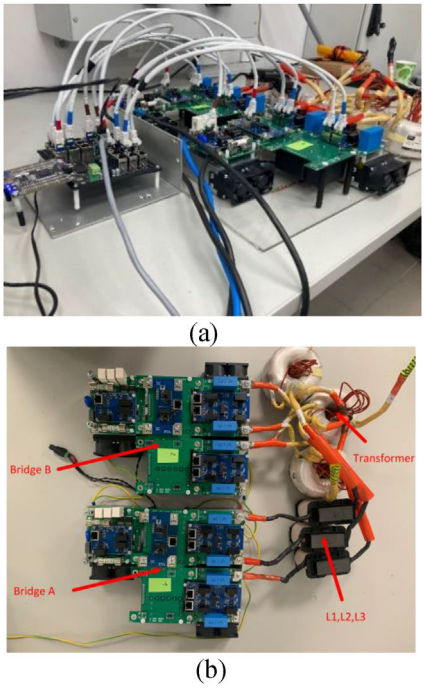

FIGURE 6 View of the laboratory setup power converter used for tests. (a) The whole converter with connected control board, (b) power hardware.

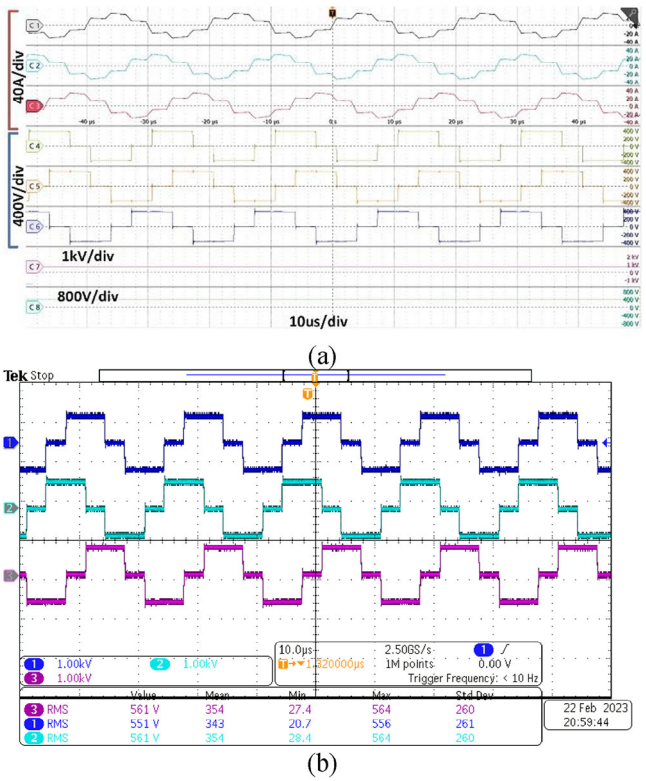

FIGURE 7 Laboratory results for Star–Star DAB 3-phase: (a) primary side results, from top: 1 to 3 phase current, 4 to 6 phase voltage, 7 DC input voltage and 8 DC output voltage, (b) secondary side phase voltages. DAB, dual active bridge.

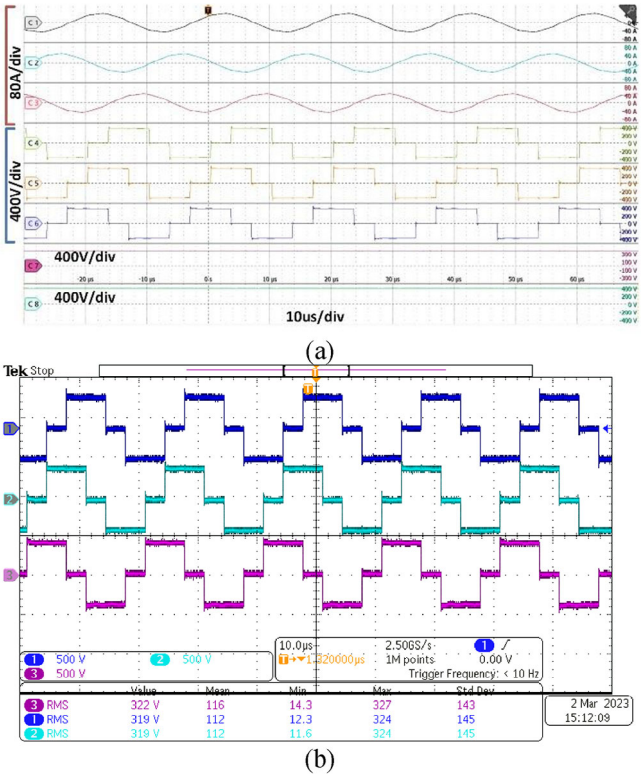

FIGURE 8 Laboratory results for Star–Delta DAB 3-phase: (a) primary side results, from top: 1 to 3 phase current, 4 to 6 phase voltage, 7 DC input voltage and 8 DC output voltage, (b) secondary side phase voltages. DAB, dual active bridge.

of phase current corresponding to the shape of phase voltages. Figure 8 presents the static results of the Star–Delta topology, showing that the phase currents have less higher harmonics and are more sinusoidal. This confirms the assumptions of the research.

Figure 9 illustrates the dynamic response comparison between the two transformer topologies under examination. The experimental assessments involved an accurate evaluation of two transformer configurations under a consistent voltage ratio, subjected to a load variation of 1 kW. Measurements were conducted for electrical values, temperature variations, and efficiency. Importantly, the series inductance remained unchanged throughout the experimental tests.

It is noteworthy that the Star–Star topology operated within a voltage range of 600 to 324 V, while the Star–Delta configuration functioned at 380 to 324 V. The observed voltage disparity is attributed to the utilization of the same transformer with distinct winding configurations. This deliberate choice mitigates challenges associated with transformer manufacturing discrepancies.

To maintain consistent phase shift values between the two configurations, the series inductance value for the Star–Delta topology underwent adjustment through multiplication by two coefficients, specifically, approximately $\sqrt{3}$ and the voltage ratio. This adjustment ensures parity with the phase shift values obtained in the Star–Star configuration. The conducted

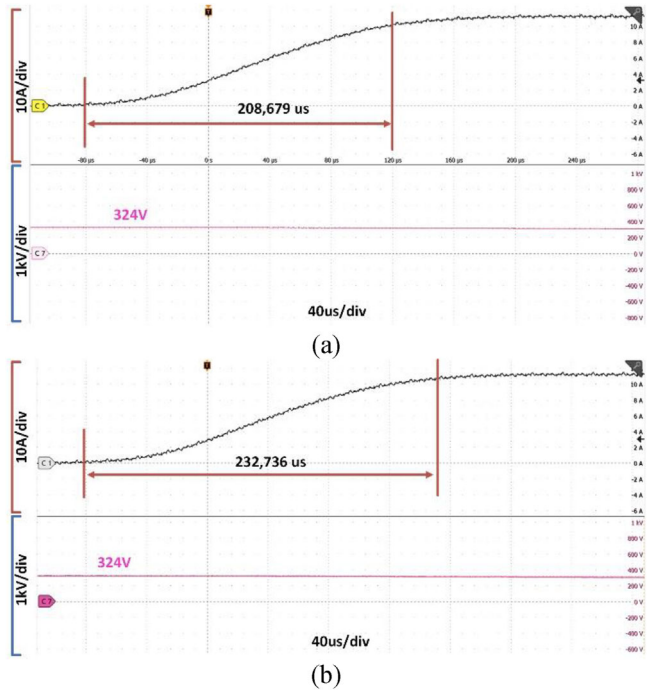

FIGURE 9 Dynamic state comparison. From top: DC output current of the DAB 3-phase and DC output voltage of the load: (a) Star–Star topology, (b) Star–Delta topology. DAB, dual active bridge.

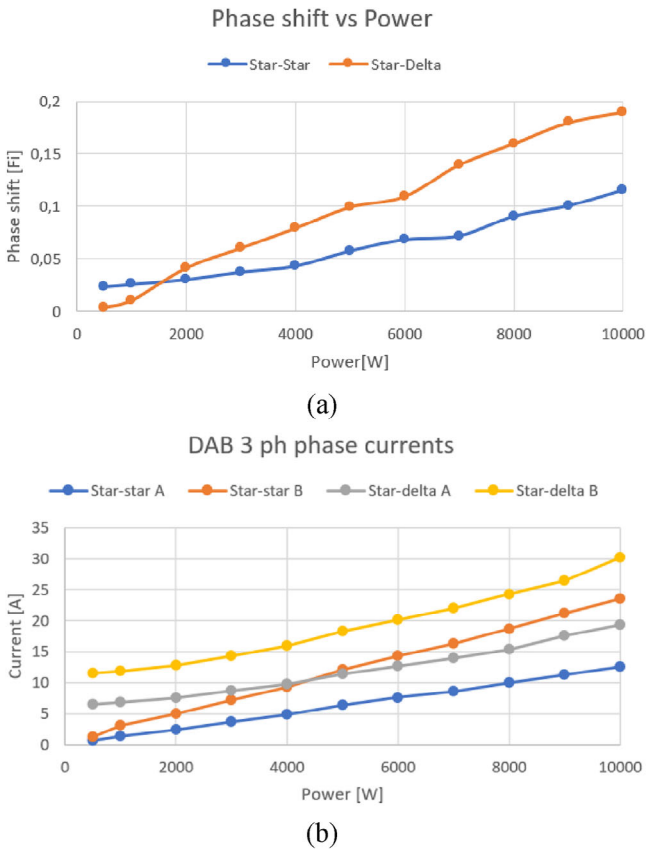

FIGURE 10 Comparison of DAB 3-phase topology. (a) Phase shift vs power, (b) phase current vs power comparison: Star–Star and Star–Delta topology. Star–Star A and Star–Star B label the phase current on both sides of transformer. DAB, dual active bridge.

tests, however, were designed to utilize identical magnetic components in varying configurations, resulting in a notable discrepancy in the phase angle, as evident in Figure 10.

It is imperative to recognize that alterations in operational parameters may introduce efficiency variations, stemming from amplified current amplitudes and consequent elevated losses in semiconductor elements. Additionally, modifications in voltage levels influence changes in phase shift. However, comparing both topologies on the same components allows for a better illustration of the differences between these topologies.

In Figures 8 and 9, a significant difference can be seen in the Star–Star and Star–Delta phase current waveforms. In the Star–Delta topology, the phase current is significantly smoothed due to the nature of the transformer topology and the reduction of current harmonic ripple. The shape of the phase current translates into the amount of EMI generated by the system. Phase current at 10 kW Star–Star: (Primary-18,75 A, Secondary-35,16 A), Star–Delta (Primary-3799 A, Secondary-2833 A).

Figure shows the difference in the shape of the phase current for DAB 3-phase in the Star–Star and Star–Delta topologies.

A mathematical analysis was carried out based on [39, 40]. On its basis, an equation for the system operation condition in the ZVS mode was derived. The laboratory results were then verified with the following conditions:

Star–Star:

$$\frac{2\pi - 3\varphi}{2\pi} \le D \le \frac{2\pi}{2\pi - 3\varphi} \; for \; 0 \le \varphi \le \frac{\pi}{3} \tag{4}$$

$$\frac{3\pi - 6\varphi}{2\pi} \le D \le \frac{2\pi}{3\pi - 6\varphi} \; for \; \frac{\pi}{3} \le \varphi \le \frac{2\pi}{3} \tag{5}$$

Star–Delta:

$$\frac{2}{3}n \le D \le 2n \; for \; 0 \le \varphi \le \frac{\pi}{6} \tag{6}$$

$$\frac{9\pi - 18\varphi}{4\pi} \le D \le \frac{4\pi}{3\pi - 6\varphi} \; for \; \frac{\pi}{6} \le \varphi \le \frac{\pi}{3} \tag{7}$$

where n is the transformer turn ratio, k_u is nU_{dc2}/U_{dc1}, P_{out} is output power and D is U_{dc1}/U_{dc2}.

In order to apply the universal ZVS characteristic for DAB applications, take into account [41]:

- Not perfect MOSFET transistor structure. The main issue here is the problem with non-linearity of the output capacitance. Because of the existence of the parasitic currents when the transistor is turned off, the ZVS area can be reduced.
- The influence of dead time values on full bridges – dead time drift effect. Dead time introduced additional phase shift drift as well as the dead time drift problem. Determining the correct dead time values should be implemented carefully. When dead time is too short, it causes the drain current not to drop to zero. Too high value of a dead time will change the ZVS range and even produce a dead band issue.
- Attention should be paid to the inaccuracies of the transformer voltage transformers and the input-to-output voltage ratio. The ideal state is when the value of this parameter is equal to one; unfortunately, this is very difficult to achieve

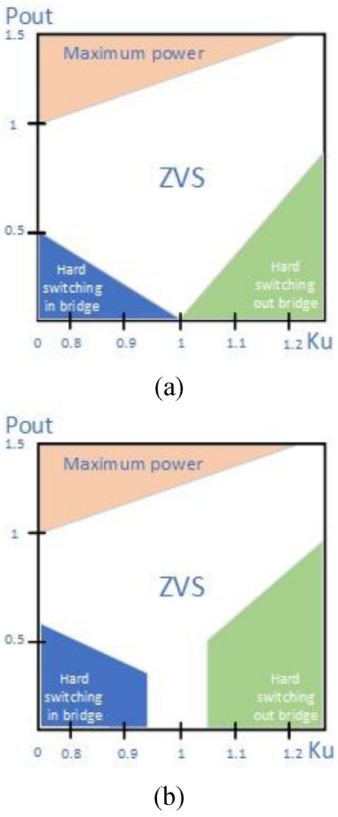

FIGURE 11 Soft switching characteristics: (a) Star–Star, (b) Star–Delta.

in practice due to problems related to control stability and resolution, oscillations of the control set value, or parameter control.

Based on the derived equations and constraints, the ZVS region shown in Figure 11 was prepared.

Upon comparing these configurations, it becomes evident that ZVS operation in the Star–Delta system is attainable at lower power levels within a specific Ku range, a feature not achievable with the Star–Star topology. Furthermore, the Star–Star topology exhibits a broader range of allowable variations in voltage ranges.

This directly translates into the performance of the presented systems under low load conditions. Consequently, the Star–Delta topology proves to be more adept at operating in the low power range. However, the assertion that the Star–Star topology boasts a significantly wider voltage range holds true. It is noteworthy that the maximum power condition remains the same for both topologies. Furthermore, the Star–Star topology exhibits ZVS characteristics remarkably similar to the DAB 1-phase topology.

In the case of the process of turning off transistors, the process of overcharging capacitances connected in parallel with the switches can be used to create soft conditions. For example, considering the diagram presented in Figure 12a, it can be assumed that after turning off the transistor T_2 and with the appropriate direction of I_o current flow, the further $I_o$flow is

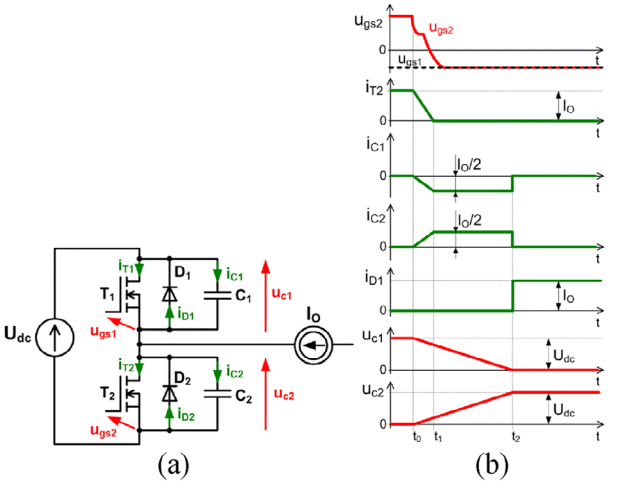

FIGURE 12 Transistor soft turn-off in an converter bridge leg with additional parallel capacitances: (a) scheme, (b) operational waveforms.

maintained by additional capacitances C_1 and C_2 (Figure 12b). As a result, compared to hard commutation, the steepness of the voltage waveforms U_{c1} and U_{c2} is reduced, which results from the process of overcharging the capacitances C_1 and C_2 by the I_o current. As a result, transistor T_2 is turned off under ZVS conditions. After the capacitance overcharging process is completed, diode D1 takes over the further conduction of the I_o current [42]. A summary and verification of the theoretical waveforms that should be in the ZVS state was also carried out, presented on Figure 13.

Further in the work, research was carried out comparing the results of the analysis with the results at the laboratory stand. An example of the presented result for one of the transistors is shown in Figure 14.

The converter operation analysis indicates that the system works in soft switching. In the state of operation with the voltage ratio equal to one, diode switching takes place in the secondary side bridge [10]. The system was checked at a low power range of 2 kW to confirm that soft switching was achieved for both topologies.

The relationship between the phase shift and transformer phase currents in both topologies is linear. This indicates that the system operates within the linear range of the output power characteristics. In the Star–Delta configuration, the phase currents are higher, primarily due to the lower input voltage and the type of connection.

The Star–Delta topology offers an extended range of phase shift angle control, thereby enhancing control accuracy. It is important to note, however, that the maximum phase angle should be carefully managed to avoid exceeding the linear section of the characteristic.

7 | EFFICIENCY COMPARISON

The tested systems are compared in Figure 15. The presented results indicate a higher efficiency of the Star–Star topology by

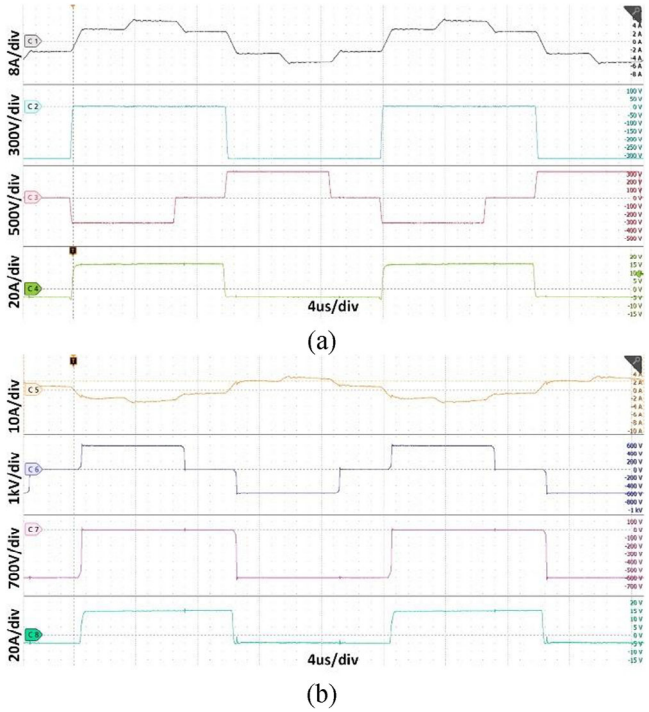

FIGURE 13 Switching condition for Star–Star topology for 2-kW load. (a) Primary side bridge. From top: phase current, source to DC+, phase voltage, gate signal of upper transistor, (b) secondary side bridge. From top: phase current, phase voltage, source to DC+, gate signal of upper transistor.

about 3%. The article [34] shows the characteristic in which the Star–Delta configuration had a slightly higher efficiency. The difference in the efficiency results obtained during the laboratory tests comes from the difference in output voltage, which for the Star–Delta topology was lower due to the design of the magnetic circuit. This difference results from the concept of the tests performed and a different approach to comparing these topologies.

Topology efficiencies have been compared with DAB 1-phase and different transformer ratio. In Figure 16 the following waveforms have been added to the presented results: comparison of the efficiency of DAB 1-phase with DAB 3-phase in the Star–Star and Star–Delta variant. The higher efficiency of the 1 phase topology results from fewer magnetic and semiconductor components. The second diagram shows the comparison of DAB 3-phase efficiency values in the Star–Star and Star–Delta topologies with the addition of the efficiency result for the reverse transformer ratio. This means the systems worked in the step-down mode.

In Figure 16b for the Star–Star topology, there is a noticeable difference in the efficiency of up to 8% between the directions of energy transmission. This is due to the fact that the system worked in mode n1 with a ratio of 1:1.82 and in mode n2 with an inverse ratio while maintaining the same voltages. The system worked in the voltage step-down mode, and in this case, the efficiency drop is not that big considering that the system worked with a voltage drop of nearly 50%. It is worth noting that increasing the voltage by 50% is also possible but has not been tested due to hardware limitations.

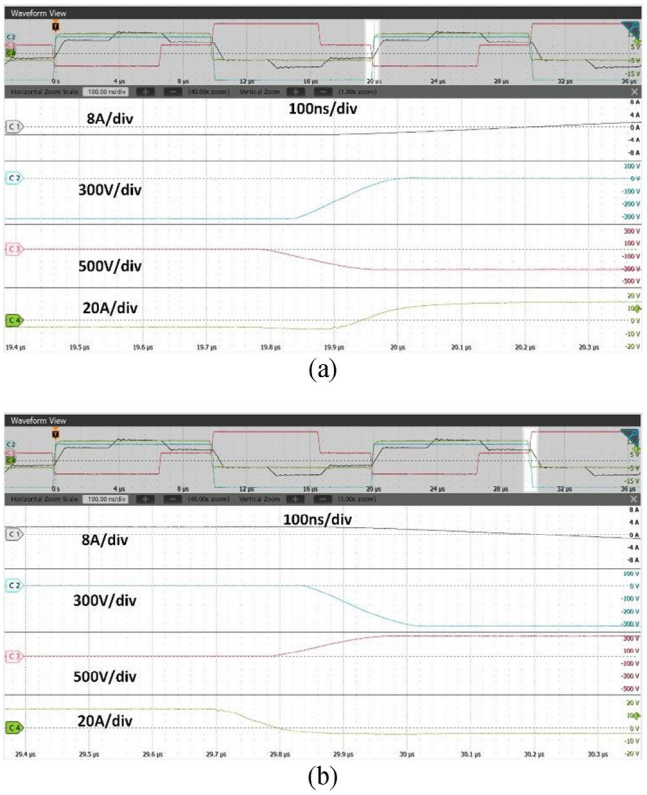

FIGURE 14 Magnified waveforms during the rising edge of the gate signal for 2-kW load. (a) Primary side bridge. From top: phase current, source to DC+, phase voltage, gate signal of upper transistor, (b) secondary side bridge. From top: phase current, phase voltage, source to DC+, gate signal of upper transistor.

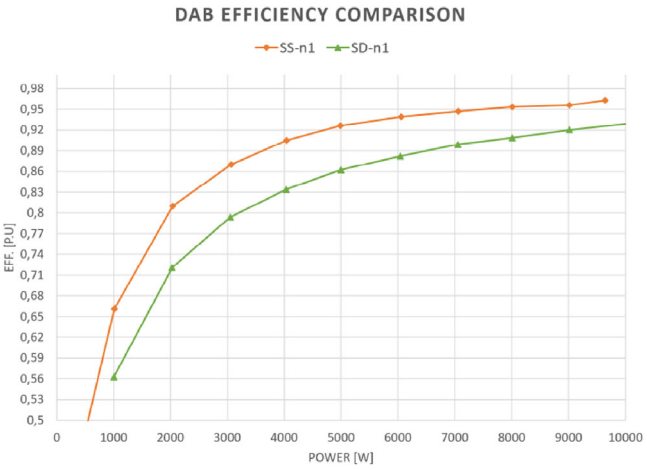

FIGURE 15 Efficiency comparison for DAB 3-phase between Star–Star and Star–Delta topology. DAB, dual active bridge.

Due to the characteristic of the transistor module used in the integrated full bridge topology, it should be noted that the losses in the system on the diodes are significant and higher than the losses on the transistors. This means that the diode losses affect the efficiency of the system depending on the direction of power transmission.

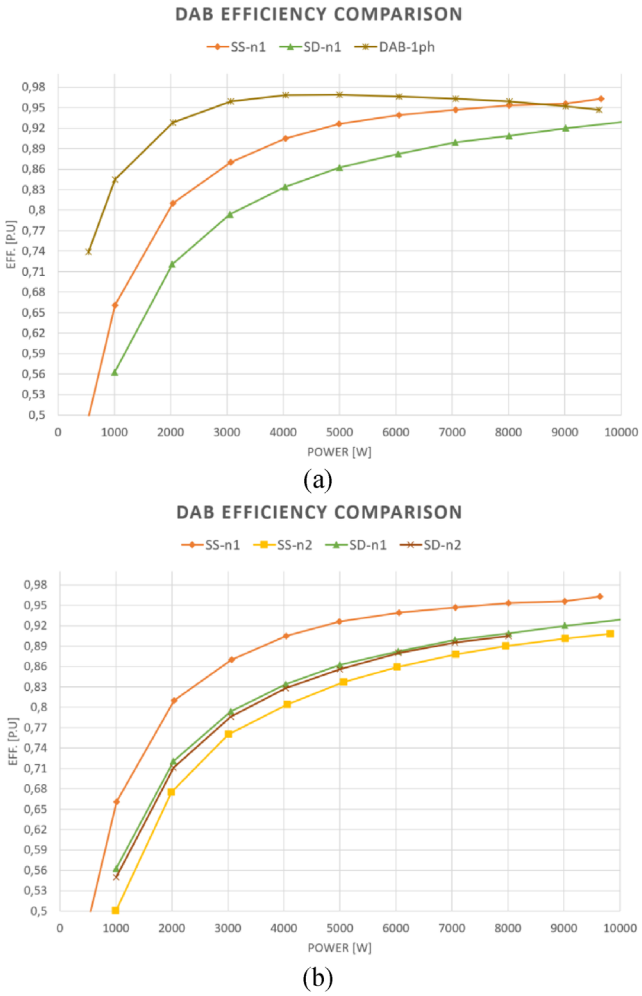

FIGURE 16 The results show the efficiency of the DAB topology in different variants. (a) Comparison of the DAB 1-phase topology with the DAB 3-phase, Star–Star, and Star–Delta topologies. (b) Comparison of DAB 3-phase Star–Star and Star–Delta in both directions. DAB, dual active bridge.

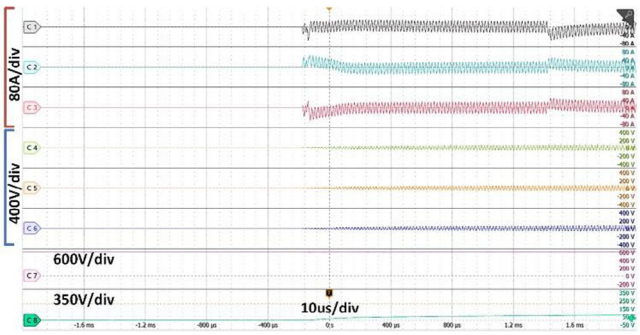

FIGURE 17 Starting inrush current for tested configurations zoom for Star–Star topology.

The starting inrush current in the tested circuit did not exceed 50 A, and was similar for the Star–Star and Star–Delta topology, result presented in Figure 17.

A comparison of the startup waveforms for a 3-ph DAB converter in the Star–Star and Star–Delta topologies is presented

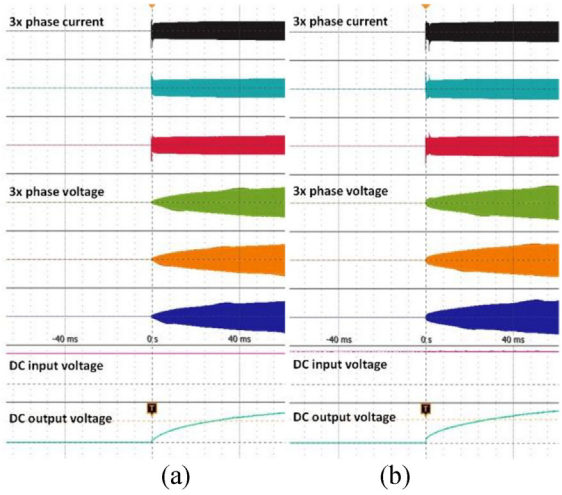

FIGURE 18 Starting inrush current for tested configurations for (a) Star–Star topology and (b) Star–Delta topology.

(Figure 18). Based on the results obtained, there were no significant differences in the overshoots of the starting currents. These results are a significant improvement compared to the results of the 1-phase DAB system.

Based on the collected results, an analysis of the harmonic components of the phase current was performed for both topologies. The summarized results are presented below in Figure 19. Based on the obtained results, it is possible to read that the harmonic level for the Star–Delta topology has been reduced by approximately 5%, results presented in Figure 19b. This result indicates a significant improvement in the emissivity of this topology. The difference in harmonic distribution for lower power is presented in Figure 19a. Total THDi values for: low powers for the Star–Star (15.7%), Star–Delta (10.4%) topologies, and high powers Star–Star (5.7%), Star–Delta (5.2%). The difference in THDi for low power is 0.7%. These results indicate that the advantage of using the Star–Delta topology becomes more pronounced as the output power increases.

8 | SUMMARY AND CONCLUSION

In the presented publication, comparative tests of the DAB 3-phase topology and comparison to DAB 1-phase were carried out. Several simulations and a test stand were provided in two variants: the Star–Star and Star–Delta. While the Star–Star topology exhibited higher efficiency, it displayed a less sinusoidal current shape.

A universal control method was employed for both 1-phase and 3-phase: Star–Star and Star–Delta variants, emphasizing the potential for simplifying large microgrid control and enhancing overall reliability. Moreover, the same magnetic components were used for testing (in a different configuration), which allowed us to compare topologies in a different way than those previously reported in the literature. This solution

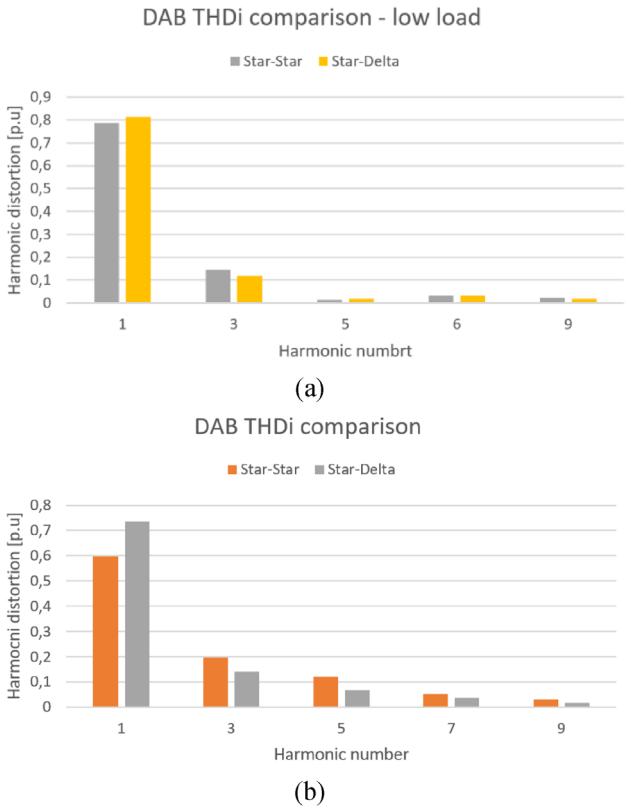

FIGURE 19 THDi comparison for Star–Star and Star–Delta topology: (a) Low load – 2 kW, (b) high load −7 kW. THDi, total harmonic distortion.

excludes differences in the implementation of magnetic circuits in comparison.

The analysis included an investigation of the ZVS region, considering non-linear phenomena and subsequently evaluating the system's performance in soft switching.

The DAB 3-phase has a lower efficiency compared to the DAB 1-phase. This is due to the number of semiconductors, the number of magnetic components, and the change in the nature of circulating currents in 3-phase magnetics. However, both topologies still have interesting properties: such as reduced EMC interference (Star–Delta) or higher efficiency (Star–Star). For this reason, we believe that both topologies can be successfully used in various applications.

In comparing DAB 3-phase topology variants, it was observed that the Star–Star configuration demonstrated superior dynamics (0.3 ms, 14% more than Star–Delta), resulting in nearly a 5% reduction in Total Harmonic Distortion (THDi) and significant emission reduction. The voltage rise difference, as measured with an ITECH laboratory load, was found to be insignificant. During performance tests, the system operated in a soft-switching region, validated through transistor switching characteristics.

The operation of the system with the reverse gear ratio and the same voltage range, and thus operation with the voltage is reduced by nearly 50%, which in turn results in a significant difference in efficiency, of even up to 8%. The presented results can be used in the design of a DC microgrid system based on multiphase DAB.

Further work will be devoted to the implementation of a universal control to a multi-module DAB converter for microgrid applications.

AUTHOR CONTRIBUTIONS

Serafin Bachman: Conceptualization; data curation; formal analysis; funding acquisition; investigation; methodology; resources; software; supervision; validation; visualization; writing—original draft; writing—review & editing. **Marek Turzyński**: Conceptualization; resources; supervision; validation. **Marek Jansinski**: Supervision.

CONFLICT OF INTEREST STATEMENT

The authors declare no conflict of interest.

FUNDING INFORMATION

This research was financed from the 'Poland-Taiwan cooperation POLTAJ VII 7th com-petition Path 1' project, co-financed by the National Center for Research and Development.

DATA AVAILABILITY STATEMENT

Data available on request from the authors

ORCID

Serafin Bachman https://orcid.org/0000-0001-9589-7612

REFERENCES

1. Turzyński, M., Bachman, S., Jasiński, M., Piasecki, S., Ryłko, M., Chiu, H.-J., Kuo, S.-H., Chang, Y.-C.: Analytical estimation of power losses in a dual active bridge converter controlled with a single-phase shift switching scheme. Energies 15, 8262 (2022). https://doi.org/10.3390/en15218262
2. Aguilar, R., Tarisciotti, L., Pereda, J.: Circulating current suppression in DAB assisted low-voltage variable frequency MMC. IEEE Trans. Ind. Appl. 58(5), 6322–6331 (2022). https://doi.org/10.1109/TIA.2022.3183959
3. Chen, Y., Chen, W., Liu, J., Tong, D., Ma, X.: EMI analysis of three-phase three-level flying capacitors diode clamped DAB converter. In: 2022 International Power Electronics Conference (IPEC-Himeji 2022- ECCE Asia), Himeji, Japan, pp. 1065–1069 (2022). https://doi.org/10.23919/IPEC-Himeji2022-ECCE53331.2022.9806945
4. Serban, E., Pondiche, C., Ordonez, M.: Analysis and design of bidirectional parallel-series DAB-based converter. IEEE Trans. Power Electron. 38(8), 10370–10382 (2023). https://doi.org/10.1109/TPEL.2023.3272336
5. Kang, K.-M., Lee, Y.-S., Lee, H., Kim, M., An, C.-G., Won, C.-Y.: Series operation method of 3-phase current-fed dual active bridge converter for battery pack charging/discharging systems. In: 2020 23rd International Conference on Electrical Machines and Systems (ICEMS), Hamamatsu, Japan, pp. 1058–1061 (2020). https://doi.org/10.23919/ICEMS50442.2020.9290902
6. Khanzadeh, B., Thiringer, T., Okazaki, Y.: Capacitor size comparison on high-power dc-dc converters with different transformer winding configurations on the ac-link. In: 2020 22nd European Conference on Power Electronics and Applications (EPE'20 ECCE Europe), pp. P.1–P.7 (2020)
7. Piasecki, S., Zaleski, J., Jasinski, M., Bachman, S., Turzyński, M.: Analysis of AC/DC/DC converter modules for direct current fast-charging applications. Energies 14, 6369 (2021). https://doi.org/10.3390/en14196369
8. Cúnico, L.M., Kirsten, A.L.: Single-phase operating modes for DC–DC three-phase dual-active-bridge with YΔ transformer. IEEE J. Emerg. Sel. Top. Power Electron. 10(4), 4845–4853 (2022). https://doi.org/10.1109/JESTPE.2022.3142686

9. Baars, N.H., Everts, J., Wijnands, C.G.E., Lomonova, E.A.: Performance evaluation of a three-phase dual active bridge DC–DC converter with different transformer winding configurations. IEEE Trans. Power Electron. 31(10), 6814–6823 (2016). https://doi.org/10.1109/TPEL.2015.2506703
10. Davoodi, A., Sadeghpour, D., Kashif, M., Albahrani, S.A., Atarodi, S.M., Zolghadri, M.: A novel transistor open-circuit fault localization scheme for three-phase dual active bridge. In: 2018 Australasian Universities Power Engineering Conference (AUPEC), Auckland, New Zealand, pp. 1–6 (2018). https://doi.org/10.1109/AUPEC.2018.8757901
11. Fritz, N., Heidenberger, D., Bündgen, D., de Doncker, R.W.: Flux control modulation for three-phase dual-active-bridge DC-DC converters. In: 2022 International Power Electronics Conference (IPEC-Himeji 2022-ECCE Asia), Himeji, Japan, pp. 1842–1849 (2022). https://doi.org/10.23919/IPEC-Himeji2022-ECCE53331.2022.9807024
12. Cúnico, L.M., Kirsten, A.L.: Improved ZVS range for three-phase dual-active-bridge converter with Wye-extended-delta transformer. IEEE Trans. Ind. Electron. 69(8), 7984–7993 (2022). https://doi.org/10.1109/TIE.2021.3102482
13. Huang, J., Li, Z., Shi, L., Wang, Y., Zhu, J.: Optimized modulation and dynamic control of a three-phase dual active bridge converter with variable duty cycles. IEEE Trans. Power Electron. 34(3), 2856–2873 (2019). https://doi.org/10.1109/TPEL.2018.2842021
14. Sun, J., Qiu, L., Liu, X., Zhang, J., Ma, J., Fang, Y.: Improved model predictive control for three-phase dual-active-bridge converters with a hybrid modulation. IEEE Trans. Power Electron. 37(4), 4050–4064 (2022). https://doi.org/10.1109/TPEL.2021.3126589
15. Jarraya, F., Zgheib, R., Abarzadeh, M., Al-Haddad, K.: Efficiency evaluation of a single phase and a three phase dual active bridge isolated DC-DC converter. In: 2019 IEEE 28th International Symposium on Industrial Electronics (ISIE), Vancouver, BC, Canada, pp. 834–839 (2019). https://doi.org/10.1109/ISIE.2019.8781482
16. Choi, H.-J., Seo, B.-G., Ryu, M.-H., Cho, Y.-P., Jung, J.-H.: Effective magnetic component design of three-phase dual-active-bridge converter for LVDC distribution system. IEEE Trans. Ind. Electron. 68(3), 1828–1840 (2021). https://doi.org/10.1109/TIE.2020.2972462
17. Noh, Y.-S., Joo, D., Hyon, B.J., Park, J.S., Kim, J.-H., Choi, J.-H.: Development of 3-phase current-fed dual active bridge converter for bi-directional battery charger application. In: 2020 IEEE Energy Conversion Congress and Exposition (ECCE), Detroit, MI, USA, pp. 2287–2290 (2020). https://doi.org/10.1109/ECCE44975.2020.9236393
18. Kondo, R., Schülting, P., Wienhausen, A.H., De Doncker, R.W.: An automated component-based hardware design of a three-phase dual-active bridge converter for a bidirectional on-board charger. In: 2020 IEEE Energy Conversion Congress and Exposition (ECCE), Detroit, MI, USA, pp. 850–857 (2020). https://doi.org/10.1109/ECCE44975.2020.9236190
19. Khanzadeh, B., Thiringer, T., Serdyuk, Y.: Analysis and improvement of harmonic content in multi-level three-phase DAB converters with different transformer windings connections. In: 2022 International Power Electronics Conference (IPEC-Himeji 2022-ECCE Asia), Himeji, Japan, pp. 2653–2658 (2022). https://doi.org/10.23919/IPEC-Himeji2022-ECCE53331.2022.9807076
20. Bündgen, D., Thönnessen, A., Fritz, N., Kamp, T., De Doncker, R.W.: Highly integrated 200 kW SiC three-phase dual-active-bridge converter with 3D-printed fluid coolers. In: 2021 IEEE 8th Workshop on Wide Bandgap Power Devices and Applications (WiPDA), Redondo Beach, CA, USA, pp. 182–187 (2021). https://doi.org/10.1109/WiPDA49284.2021.9645076
21. Dworakowski, P., Wilk, A., Michna, M., Lefebvre, B., Lagier, T.: 3-phase medium frequency transformer for a 100 kW 1.2 kV 20 kHz Dual Active Bridge converter. In: IECON 2019 - 45th Annual Conference of the IEEE Industrial Electronics Society, Lisbon, Portugal, pp. 4071–4076 (2019). https://doi.org/10.1109/IECON.2019.8926695
22. Liu, P., Chen, C., Duan, S., Zhu, W.: Dual phase-shifted modulation strategy for the three-level dual active bridge DC–DC converter. IEEE Trans. Ind. Electron. 64(10), 7819–7830 (2017). https://doi.org/10.1109/TIE.2017.2696488
23. Cui, Y., Wang, D., Emadi, A.: Three-phase dual active bridge converter design considerations. In: IECON 2017 - 43rd Annual Conference of the IEEE Industrial Electronics Society, Beijing, China, pp. 4696–4701 (2017). https://doi.org/10.1109/IECON.2017.8216809
24. Hu, J., Cui, S., De Doncker, R.W.: DC fault ride-through of a three-phase dual-active bridge converter for DC grids. In: 2018 International Power Electronics Conference (IPEC-Niigata 2018 -ECCE Asia), Niigata, Japan, pp. 2250–2256 (2018). https://doi.org/10.23919/IPEC.2018.8507672
25. Tripathi, A., et al.: MVDC microgrids enabled by 15 kV SiC IGBT based flexible three phase dual active bridge isolated DC-DC converter. In: 2015 IEEE Energy Conversion Congress and Exposition (ECCE), Montreal, QC, Canada, pp. 5708–5715 (2015). https://doi.org/10.1109/ECCE.2015.7310462
26. Gomez, R.A., Porras, D.A., Oggier, G., Balda, J.C., Zhao, Y.: Three phase dual active bridges with integrated series inductance using 10-kV SiC MOSFETs for medium-voltage grid applications. In: 2023 IEEE Applied Power Electronics Conference and Exposition (APEC), Orlando, FL, USA, pp. 2327–2332 (2023). https://doi.org/10.1109/APEC43580.2023.10131458
27. Waltrich, G., Hendrix, M.A.M., Duarte, J.L.: Three-phase bidirectional DC/DC converter with six inverter legs in parallel for EV applications. IEEE Trans. Ind. Electron. 63(3), 1372–1384 (2016). https://doi.org/10.1109/TIE.2015.2494001
28. Sal y Rosas, D., Chavez, D., Frey, D., Ferrieux, J.-P.: Single-stage isolated and bidirectional three-phase series-resonant AC–DC converter: Modulation for active and reactive power control. Energies 15, 8070 (2022). https://doi.org/10.3390/en15218070
29. Núñez, R.O., Oggier, G.G., Botterón, F., Garcia, G.O.: Analysis of the transformer influence on a three-phase dual active bridge DC-DC converter. IEEE Lat. Am. Trans. 14(7), 3048–3055 (2016). https://doi.org/10.1109/TLA.2016.7587601
30. Aouiti, A., Soyed, A., Bacha, F.: Control and study of the bidirectional three phase DAB converter. In: 2022 8th International Conference on Control, Decision and Information Technologies (CoDIT), Istanbul, Turkey, pp. 1008–1013 (2022). https://doi.org/10.1109/CoDIT55151.2022.9804020
31. de Oliveira, E.F., da Silva Filho, O.C., Yu, X., Zacharias, P.: Small-signal model and control design considerations for three-phase dual active bridge converters. In: PCIM Europe digital days 2021, International Exhibition and Conference for Power Electronics, Intelligent Motion, Renewable Energy and Energy Management, Online, 2021, pp. 1–8 (2021)
32. Choi, H.-J., Park, H.-P., Kim, M.-A., Sang-Gyu, C., Lee, C.-U., Jung, J.-H.: Modulation strategy of three-phase dual-active-bridge converter using SiC-MOSFET for improving light load condition. In: 2019 IEEE Workshop on Wide Bandgap Power Devices and Applications in Asia (WiPDA Asia), Taipei, Taiwan, pp. 1–5 (2019). https://doi.org/10.1109/WiPDAAsia.2019.8760335
33. Núñez, R.O., Oggier, G.G., Botterón, F., García, G.O.: Three-phase dual active bridge DC-DC converter: Comparison between YY and AY transformer connections. In: 2015 XVI Workshop on Information Processing and Control (RPIC), Cordoba, Argentina, pp. 1–6 (2015) https://doi.org/10.1109/RPIC.2015.7497141
34. Baars, N., Everts, J., Wijnands, K., Lomonova, E.: Impact of different transformer-winding configurations on the performance of a three-phase dual active bridge DC-DC converter. In: 2015 IEEE Energy Conversion Congress and Exposition (ECCE), Montreal, QC, Canada, pp. 637–644 (2015). https://doi.org/10.1109/ECCE.2015.7309749
35. Baars, N.H., Wijnands, C.G.E., Everts, J.: A three-level three-phase dual active bridge DC-DC converter with a star-delta connected transformer. In: 2016 IEEE Vehicle Power and Propulsion Conference (VPPC), Hangzhou, China, pp. 1–6 (2016). https://doi.org/10.1109/VPPC.2016.7791601
36. Noh, Y.-S., Hyun, S.-W., Hyon, B.J., Kim, J.-H., Choi, J.-H.: Control method to increase efficiency of 3-phase current-fed dual active bridge converter. In: 2018 21st International Conference on Electrical Machines and Systems (ICEMS), Jeju, South Korea, pp. 2157–2160 (2018). https://doi.org/10.23919/ICEMS.2018.8549322
37. Le, T.-T., Nguyen, M.-K., Wang, C., Choi, S.: Fault-tolerant control of three-phase bidirectional current-fed dual active bridge DC-DC converter. In: 2021 IEEE Transportation Electrification Conference & Expo

(ITEC), Chicago, IL, USA, pp. 360–363 (2021). https://doi.org/10.1109/ITEC51675.2021.9490140
38. Bachman, S., Turzński, M., Jasiński, M.: Modern Control Strategy of Bidirectional DAB Converter with Consideration of Control Nonlinearity. SENE, Łódź (2023)
39. Huang, J., Wang, Y., Li, Z., Jiang, Y., Lei, W.: Simultaneous PWM control to operate the three-phase dual active bridge converter under soft switching in the whole load range. In: 2015 IEEE Applied Power Electronics Conference and Exposition (APEC), Charlotte, NC, USA, pp. 2885–2891 (2015). https://doi.org/10.1109/APEC.2015.7104760
40. van Hoek, H., Ferreira, J.A., de Doncker, R.W.: Design and operation considerations of three-phase dual active bridge converters for low-power applications with wide voltage ranges (2017)
41. Jin, H., Pei, Y., Wang, L., Wen, J., Yang, C., Dong, X.: Achieving rated power and ZVS for dual active bridge converter considering the interaction of nonidealities. IEEE Trans. Ind. Electron. 70(8), 7867–7878 (2023). https://doi.org/10.1109/TIE.2022.3232662
42. Turzyński, M., Bachman, S., Jasiński, M., Piasecki, S., Ryłko, M., Chiu, H.-J., Kuo, S.-H., Chang, Y.-C.: Analytical estimation of power losses in a dual active bridge converter controlled with a single-phase shift switching scheme. Energies 15, 8262 (2022). https://doi.org/10.3390/en15218262

How to cite this article: Bachman, S., Turzyński, M., Jasiński, M.: Comparative analysis of three-phase dual active bridge converter with different transformer topology and modern universal control for DC microgrids. IET Power Electron. 1–13 (2024). https://doi.org/10.1049/pel2.12647